Contribution of water-limited ecoregions to their own supply of rainfall

2016 Environ. Res. Lett. 11 124007

(http://iopscience.iop.org/1748-9326/11/12/124007)

Environmental Research Letters

LETTER

Contribution of water-limited ecoregions to their own supply of rainfall

Diego G Miralles[1,2], **Raquel Nieto**[3], **Nathan G McDowell**[4], **Wouter A Dorigo**[5,2], **Niko EC Verhoest**[2], **Yi Y Liu**[6,7], **Adriaan J Teuling**[8], **A Johannes Dolman**[1], **Stephen P Good**[9] **and Luis Gimeno**[3]

[1] Department of Earth Sciences, VU University Amsterdam, Amsterdam, 1081-HV, Amsterdam, The Netherlands
[2] Laboratory of Hydrology and Water Management, Ghent University, B-9000, Ghent, Belgium
[3] EPhysLab, Department of Applied Physics, Faculty of Science, Universidad de Vigo, ES-32004, Ourense, Spain
[4] Los Alamos National Laboratory, Earth and Environmental Sciences Division, Los Alamos, NM 87545, USA
[5] Department of Geodesy and Geoinformation, Vienna University of Technology, Vienna, 1040, Austria
[6] ARC Centre of Excellence for Climate Systems Science and Climate Change Research Centre, University of New South Wales, Sydney, 2052, Australia
[7] School of Geography and Remote Sensing, Nanjing University of Information Science and Technology, Nanjing, 210044, People's Republic of China
[8] Hydrology and Quantitative Water Management Group, Wageningen University, 6708-PB, Wageningen, The Netherlands
[9] Department of Biological and Ecological Engineering, Oregon State University, Corvallis, OR 97331, USA

E-mail: Diego.Miralles@VU.nl

Keywords: precipitation recycling, drought, water-limited regions, land–atmospheric feedbacks, evaporation, vegetation optical depth, global ecohydrology

Supplementary material for this article is available online

OPEN ACCESS

RECEIVED
27 May 2016

REVISED
31 October 2016

ACCEPTED FOR PUBLICATION
16 November 2016

PUBLISHED
28 November 2016

Abstract

The occurrence of wet and dry growing seasons in water-limited regions remains poorly understood, partly due to the complex role that these regions play in the genesis of their own rainfall. This limits the predictability of global carbon and water budgets, and hinders the regional management of natural resources. Using novel satellite observations and atmospheric trajectory modelling, we unravel the origin and immediate drivers of growing-season precipitation, and the extent to which ecoregions themselves contribute to their own supply of rainfall. Results show that persistent anomalies in growing-season precipitation—and subsequent biomass anomalies—are caused by a complex interplay of land and ocean evaporation, air circulation and local atmospheric stability changes. For regions such as the Kalahari and Australia, the volumes of moisture recycling decline in dry years, providing a positive feedback that intensifies dry conditions. However, recycling ratios increase up to 40%, pointing to the crucial role of these regions in generating their own supply of rainfall; transpiration in periods of water stress allows vegetation to partly offset the decrease in regional precipitation. Findings highlight the need to adequately represent vegetation–atmosphere feedbacks in models to predict biomass changes and to simulate the fate of water-limited regions in our warming climate.

1. Introduction

Drylands cover 40% of the continental surface and sustain almost one half of world's population (White and Nackoney 2003). They include water-limited ecoregions such as shrublands, savannas or steppes. Annual precipitation is low and usually concentrated in just a few months, between prolonged periods of combined rainfall scarcity and high atmospheric demand for water (Rodriguez-Iturbe *et al* 2001, Guswa *et al* 2004). In these dry regions, the overall health of vegetation, the survival of certain species and the amount of aboveground biomass are largely dependent on water availability during the growing season, which is strongly controlled by precipitation. Meanwhile, the role of drylands in shaping Earth system dynamics cannot be overstated: recent studies have revealed that global declines in primary productivity

and vegetation water use are linked to the occurrence of precipitation anomalies in dry regions (Miralles *et al* 2014b, Poulter *et al* 2014, Ahlström *et al* 2015).

The precipitation supply to any ecoregion is fundamentally driven by changes in atmospheric moisture content and the stability of the atmosphere (Gimeno *et al* 2010a, Dirmeyer *et al* 2014, Schubert *et al* 2016), letting aside the influence of more localised factors such as the emission of aerosols during wildfires (Ramanathan 2001). The atmospheric moisture content over the ecoregion is a function of the volume of water evaporated from the ecoregion itself and from neighbouring or remote (ocean and land) areas, and depends on whether this evaporated moisture is driven by winds into the ecoregion (i.e. atmospheric circulation). Finally, convective and synoptic atmospheric instability will determine whether the advected (and locally-generated) atmospheric moisture does in fact precipitate. In that sense, the evaporation happening within an ecoregion—mostly through transpiration (Jasechko *et al* 2013, Miralles *et al* 2016)—impacts the ecoregion's supply of precipitation: local evaporation not only increases the atmospheric moisture content, but it also alters the convective stability of the lower atmosphere (Betts and Ball 1998, Koster *et al* 2004, Taylor and Ellis 2006). Consequently, soil moisture and vegetation may influence the ecoregion's input of precipitation through their effects on evaporation. This also implies that soil desiccation or land use change within the ecoregion—but also in remote upwind areas—can in turn have significant effects on local precipitation (Keys *et al* 2012, Bagley *et al* 2014, Dirmeyer *et al* 2014, Spracklen and Garcia-Carreras 2015).

To date, most studies of global precipitation–vegetation dynamics have focused on describing or quantifying their local correlation (Nemani 2003, Zhao and Running 2010, Wu *et al* 2015, Seddon *et al* 2016). Yet, our understanding remains limited in regards to the mechanisms responsible for the occurrence of wet and dry growing seasons, how these affect vegetation over large scales, and what the role of vegetation itself is in either buffering or intensifying these conditions. Nonetheless, progress has been made on understanding the large-scale ocean and atmospheric patterns that ultimately affect inter-annual precipitation variability (Schubert *et al* 2016), but the immediate (or proximate) factors driving this variability in the most water-dependent regions on Earth remain elusive, including the influence that the ecoregions themselves play on their own supply of rainfall. This is partly due to the complexity of vegetation impacts on climate (Bonan 2008), the difficulties to realistically represent land–atmospheric interactions in models (Seneviratne *et al* 2010), and the impossibility to quantify these causal relationships based on observations only (Miralles *et al* 2014a, Casagrande *et al* 2015).

Here, we identify the major global water-limited ecoregions on Earth, to then provide novel understanding of the immediate mechanisms behind the anomalies in their growing-season precipitation and the ecoregions' response and contribution to these anomalies. For this purpose, we use a new vegetation optical depth (VOD) satellite product and global meteorological observations, which are combined with 3D Lagrangian modelling (Stohl *et al* 1998, Seibert and Frank 2004), allowing us to track the water vapour entering these regions. We explore anomalies in precipitation volumes, origin of advected moisture, local precipitation recycling, and impact of water scarcity on vegetation. Three immediate (or proximate) drivers of wet and dry growing seasons are evaluated independently: local and remote evaporation anomalies, fluctuations in atmospheric circulation, and persistent synoptic and convective stability conditions. Given the high vulnerability of water-limited ecoregions to changes in water supply (Manfreda and Caylor 2013, Seddon *et al* 2016) and the vast population they sustain (White and Nackoney 2003), understanding the interplay among these immediate drivers of precipitation is critical to predict their ecosystem services, adapt to future changes, and narrow down uncertainties in global carbon, energy and water budgets (Poulter *et al* 2014, Miralles *et al* 2014b, Ahlström *et al* 2015).

2. Materials and methods

2.1. Data sets

Our analysis relies on the multi-decadal record of VOD recently developed by Liu *et al* (2011) and updated by Liu *et al* (2015), which is based on a wide range of passive microwave satellite observations. This data set is used to identify global water-limited ecoregions—for which our atmospheric vapour trajectories model will be run afterwards—and to quantify the changes in the state of vegetation between wet and dry years. VOD is a close proxy for the water content in vegetation, including both leaf and woody components, and it is strongly linked to aboveground biomass density and vegetation activity (Andela *et al* 2013, Liu *et al* 2015). Apart from being more easily interpretable than traditional greenness indices, it is also insensitive to sun-sensor geometry and has a minimal sensitivity to atmospheric conditions (Liu *et al* 2011). The VOD by Liu *et al* (2011) is based on the application of the land parameter retrieval model (Owe *et al* 2008) to passive microwave observations from the scanning multichannel microwave radiometer, the special sensor microwave imager (SSM/I), the tropical rainfall measuring mission microwave imager (TMI) and the advanced microwave scanning radiometer-Earth observing system (AMSR-E).

To complement the analysis, we use normalized difference vegetation index (NDVI) data coming from the global inventory monitoring and modeling system (GIMMS) third generation (3g) data set (Tucker

et al 2005), which is based on optical data from the advanced very high resolution radiometer (AVHRR). In addition, precipitation, evaporation and atmospheric stability data are used to investigate the differences in the origin and volumes of precipitation between wet and dry years. Precipitation observations are obtained from the Climate Research Unit (CRU) 3.10 gauge-based product (Harris *et al* 2013). Land evaporation data (including transpiration) are taken from the satellite observation-based global evaporation Amsterdam model (GLEAM, Miralles *et al* 2011), and ocean evaporation from the satellite observation-based OAFlux data set (Yu 2007). Background atmospheric stability is assessed using monthly estimates vertical wind velocity (ω) at 500 hPa and convective available potential energy (CAPE), both derived from the ERA-Interim reanalysis (Dee *et al* 2011). All data sets are re-gridded to a common 0.25° spatial resolution and aggregated to monthly temporal resolutions. Monthly anomalies are then calculated by subtracting the corresponding month-of-the-year mean considering the multi-annual (1980–2011) record.

2.2. Atmospheric trajectory model

The Lagrangian particle dispersion model FLEXPART v9.0 (Stohl *et al* 1998, Seibert and Frank 2004) is used to trace water vapour trajectories and quantify moisture sources. FLEXPART is here constrained by wind and specific humidity data from ERA-Interim, as in recent applications of the model dedicated to investigate water vapour trajectories (Drumond *et al* 2014, Nieto *et al* 2014, Pampuch *et al* 2016). The atmosphere is divided into two million air particles that are moved by 3D winds. The model calculates increases and decreases in moisture along a given trajectory based on differentials of specific humidity in time, and records these changes in specific humidity and the 3D coordinates of all particles every 6 h. By summing all the increases and decreases of moisture over a given grid cell, the difference between evaporation and precipitation ($E - P$) can be obtained, which is then integrated over the average atmospheric residence time. A review of the advantages, limitations and uncertainties of different moisture transport models, including FLEXPART, can be found in Gimeno *et al* (2012).

3. Approach

3.1. Identification of water-limited ecoregions

Based on the VOD data and precipitation observations from CRU, figure 1(c) delineates the ten major water-dependent ecoregions on Earth—here, the concept of 'ecoregion' by Olson and Dinerstein (2001) is loosely used to refer to large (>100 000 km^2) contiguous geographical areas of similar climate and vegetation conditions. The identification of these water-limited ecoregions is based on clustering neighbouring pixels following two inclusive criteria: (a) the expected timing of the annual peak in VOD, as revealed from the monthly climatology calculated based on 1980–2011, should be similar (i.e. ±1 month) for all pixels in the area (see figure 1(a)), and (b) the Pearson's correlation between the annual value of VOD at that seasonal peak, and the cumulative precipitation during the antecedent three months should be statistically significant ($p < 0.01$) and larger than 0.5 (see figure 1(b)). Hereafter, we refer to these three months prior to the seasonal peak in VOD as 'growing season'. Correlations to precipitation were calculated by considering other antecedent periods ranging from 1 to 10 months, and the final choice of three months was adopted for it yields the maximum average correlations globally (not shown). We note that this definition of a constant-length growing season differs from others found in literature, yet it facilitates the study of atmospheric vapour trajectories (see section 3.2). We note as well, that the inclusion of water-limited ecoregions in figure 1(c) is not aiming to be exhaustive, and that several other areas that fulfil the two above-mentioned criteria are not further analysed with FLEXPART due to their smaller size, their less clustered geographical distribution, or their proximity to larger water-limited ecoregions; examples are the Russian steppe or Southeastern Australia (see figure 1(b)).

Overall, we identify ten major ecoregions, from West to East (figure 1(c)): (1) Chihuahuan Desert, (2) Pampas, (3) Caatinga, (4) West Sudanian savanna, (5) Kalahari Desert, (6) East Sudanian savanna, (7) Serengeti bushland, (8) Mongolian steppe, (9) Central Australia and (10) Northern Australia. The general characteristics of these ecoregions are summarised in supplementary table A1.

3.2. Estimation of precipitation origin for each ecoregion

The precipitation origin is calculated following three sequential steps. First, from each water-stressed ecoregion in figure 1(c), the FLEXPART model is run backward (Nieto *et al* 2014) to simulate the origin of the air particles entering the ecoregion's atmosphere during the growing season. As mentioned above, the length of the growing season is considered constant and equal to the three months prior to each regions' seasonal peak in VOD (see supplementary table A1). The common time length for all ecoregions allows their results to be inter-comparable, and by considering a short enough period, we circumvent the confounding effect of the seasonal cycle of atmospheric circulation. Backward runs are analysed separately for the five years of higher and lower peak in vegetation water content (i.e. VOD) during the 1980–2011 period, hereafter referred to as 'wet years' and 'dry years' (respectively). This allows us to identify inter-annual anomalies in the trajectories of air particles

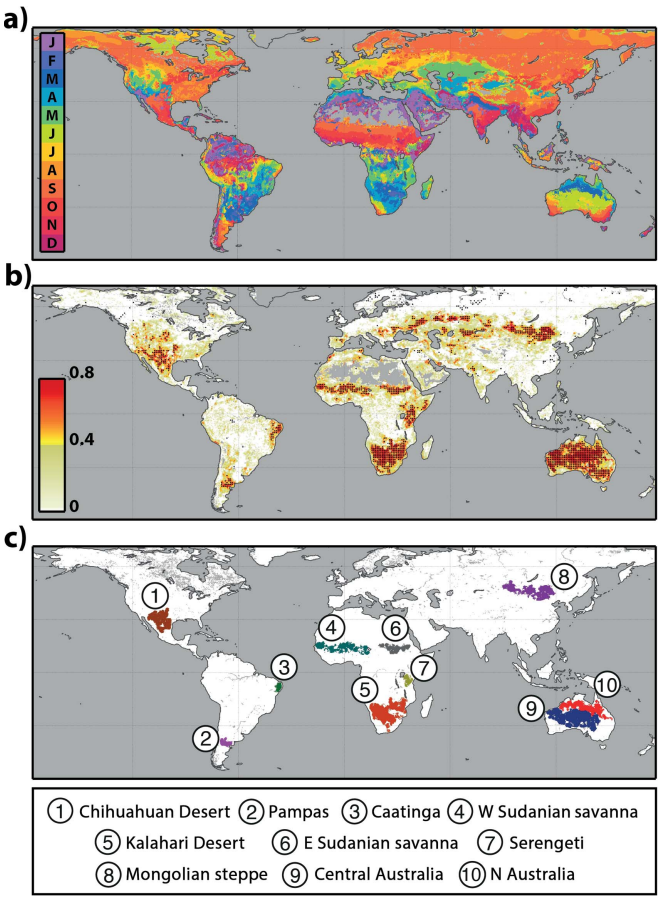

Figure 1. Identification of water-limited ecoregions. (a) Month of the year in which vegetation peaks according to the climatology of VOD. (b) Pearson's correlation coefficient between the values of VOD at the month of climatological maximum (see figure 1(a)) and the cumulative precipitation during the previous three months (here referred to as 'growing season'). Time series are linearly detrended to avoid spurious correlations due to, e.g., coinciding long-term wetting and greening trends. Results are based on CRU monthly precipitation (Harris *et al* 2013) and the VOD data by Liu *et al* (2011) for the period 1980–2011. Dotting indicates statistical significance ($p < 0.01$, calculated using a *t*-test), with the dotting net represented at 1° resolution to aid visualisation. (c) Water-limited ecoregions, delineated based on figure 1(a) (aiming to group regions that share the timing of the seasonal vegetation peak ±1 month) and figure 1(b) (using a minimum threshold of 0.5 Pearson's correlation).

entering the ecoregion, and in the gain of water vapour through these trajectories. An optimal lifetime of vapour in the atmosphere needs to be considered in the calculation of back-trajectories with FLEXPART; for each region, this lifetime (in number of days) is optimised by executing the model sequentially for a range of possible lifetime values, and then selecting the number of days that minimises the absolute differences between the precipitation simulated by FLEXPART and the CRU observations for each ecoregion (see supplementary table A1 for the resulting lifetimes).

Second, once the vapour source region has been identified for each ecoregion, FLEXPART is run forward from these source regions. Only the fraction of them contributing to 90% of the water vapour entering the ecoregions is considered, in order to exclude remote source regions with very small moisture contributions (Drumond *et al* 2014). This forward run yields the volumes of rain falling in each ecoregion during the corresponding growing season. Therefore, while the backward run only identifies the origin of the moisture entering the ecoregion, the forward run reveals whether the moisture gained over that trajectory does in fact precipitate in the ecoregion, which would finally depend on atmospheric stability. This forward run is done for wet and dry years independently, and separately for: (a) the ocean pixels within the source region, (b) the land pixels within the source region but outside the ecoregion, and (c) the ecoregion itself. This enables us to discern whether precipitation falling in the ecoregion during the growing season is of oceanic or terrestrial origin, and if the latter, whether or not it originates from the ecoregion itself (see figure 2).

Third, the volumes of precipitation simulated by the forward runs of FLEXPART are scaled to match monthly CRU observations, while maintaining the FLEXPART-derived ratios of ocean and terrestrial origin. The resulting volumes of precipitation from land and oceanic origin are spatially distributed across the pixels in the source region using the results from the backward runs. This allows us to spatially map the origin of the precipitation volumes falling into each

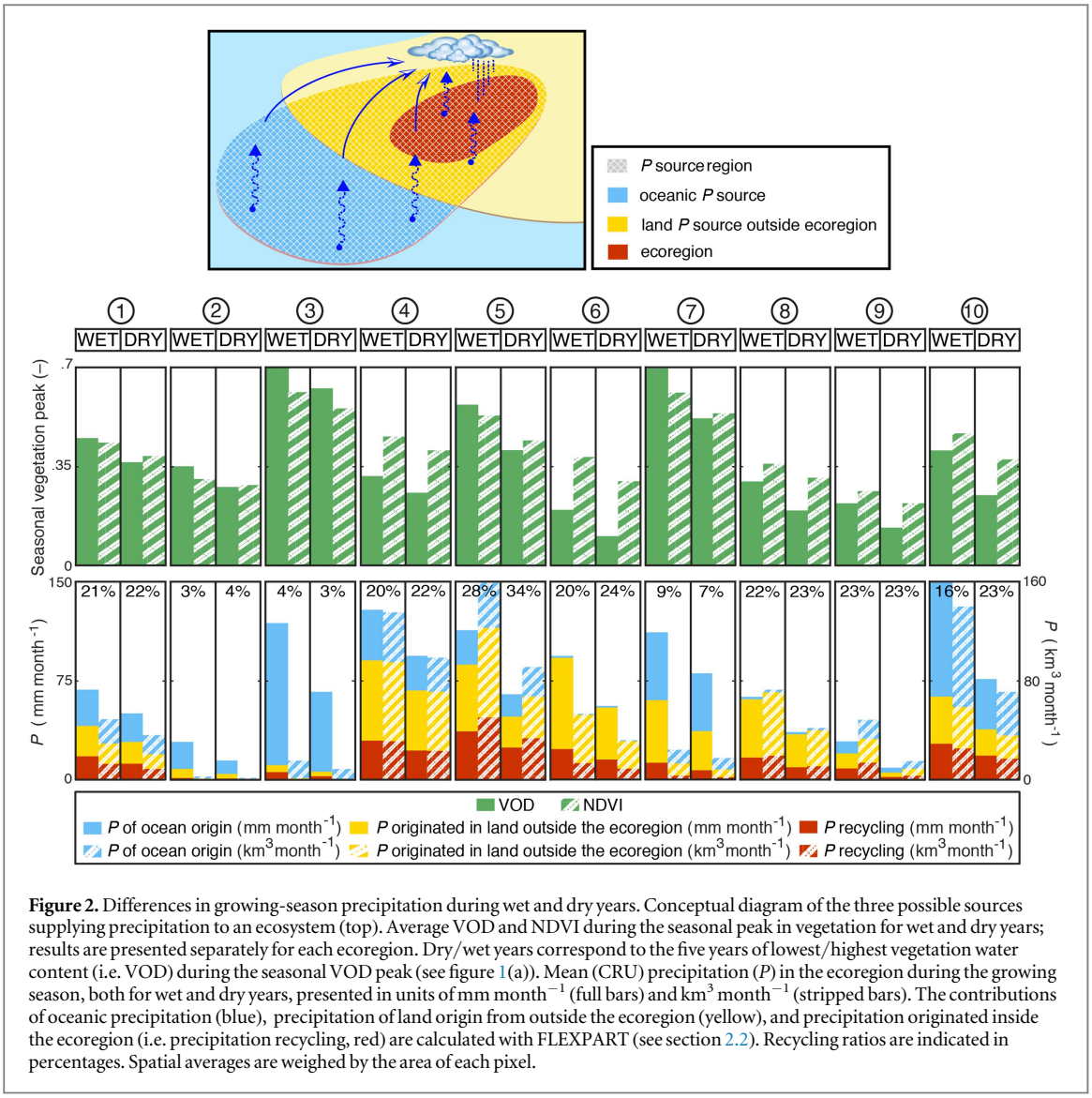

Figure 2. Differences in growing-season precipitation during wet and dry years. Conceptual diagram of the three possible sources supplying precipitation to an ecosystem (top). Average VOD and NDVI during the seasonal peak in vegetation for wet and dry years; results are presented separately for each ecoregion. Dry/wet years correspond to the five years of lowest/highest vegetation water content (i.e. VOD) during the seasonal VOD peak (see figure 1(a)). Mean (CRU) precipitation (P) in the ecoregion during the growing season, both for wet and dry years, presented in units of mm month^{-1} (full bars) and km^3 month^{-1} (stripped bars). The contributions of oceanic precipitation (blue), precipitation of land origin from outside the ecoregion (yellow), and precipitation originated inside the ecoregion (i.e. precipitation recycling, red) are calculated with FLEXPART (see section 2.2). Recycling ratios are indicated in percentages. Spatial averages are weighed by the area of each pixel.

ecoregion, showing the specific contribution of each source pixel to these volumes (see e.g. figure 3). Finally, precipitation recycling ratios for each water-stressed ecoregion are calculated as the ratio of the precipitation generated within the ecoregion, over the total input of precipitation. This ratio is then multiplied by 0.9 to account for the fact that the source region used in forward simulations includes only 90% of the particles bringing moisture into the ecoregion, and that the ecoregion is always contained within that 90%. These recycling ratios are then averaged for wet and dry years separately, and for each corresponding ecoregion, as shown in figure 2.

4. Results

4.1. Precipitation origin during wet and dry growing seasons

Based on the VOD data and CRU precipitation, figure 1(c) delineates the ten major global water-limited ecoregions on Earth. For all these regions the seasonal peak in VOD is significantly ($p < 0.01$) and positively correlated ($R \geqslant 0.5$) to the cumulative precipitation occurring in the prior three months (figure 1(b)). Independently of the magnitude of precipitation anomalies, comparatively high VOD values are found in the more tropical Caatinga and Serengeti, and relatively low VOD values are found in the more arid East Sudanian savanna and Central Australia (figure 2), which is in agreement with the results by Liu *et al* (2013). Most regions experience pronounced differences in VOD between wet and dry years, especially the Kalahari, Serengeti, East Sudanian savanna and Northern Australia, likely due to the strong differences in precipitation volumes between wet and dry years in these regions (figure 2) and a potentially high sensitivity of vegetation to those differences. Analogous inter-region and inter-period variability is found when using vegetation greenness (NDVI) instead of VOD (figure 2). The precipitation during the growing season is markedly lower for dry years in all ecoregions, but the response of vegetation is not equal for all of them: figure 2 reveals important inter-region differences that may reflect the presence

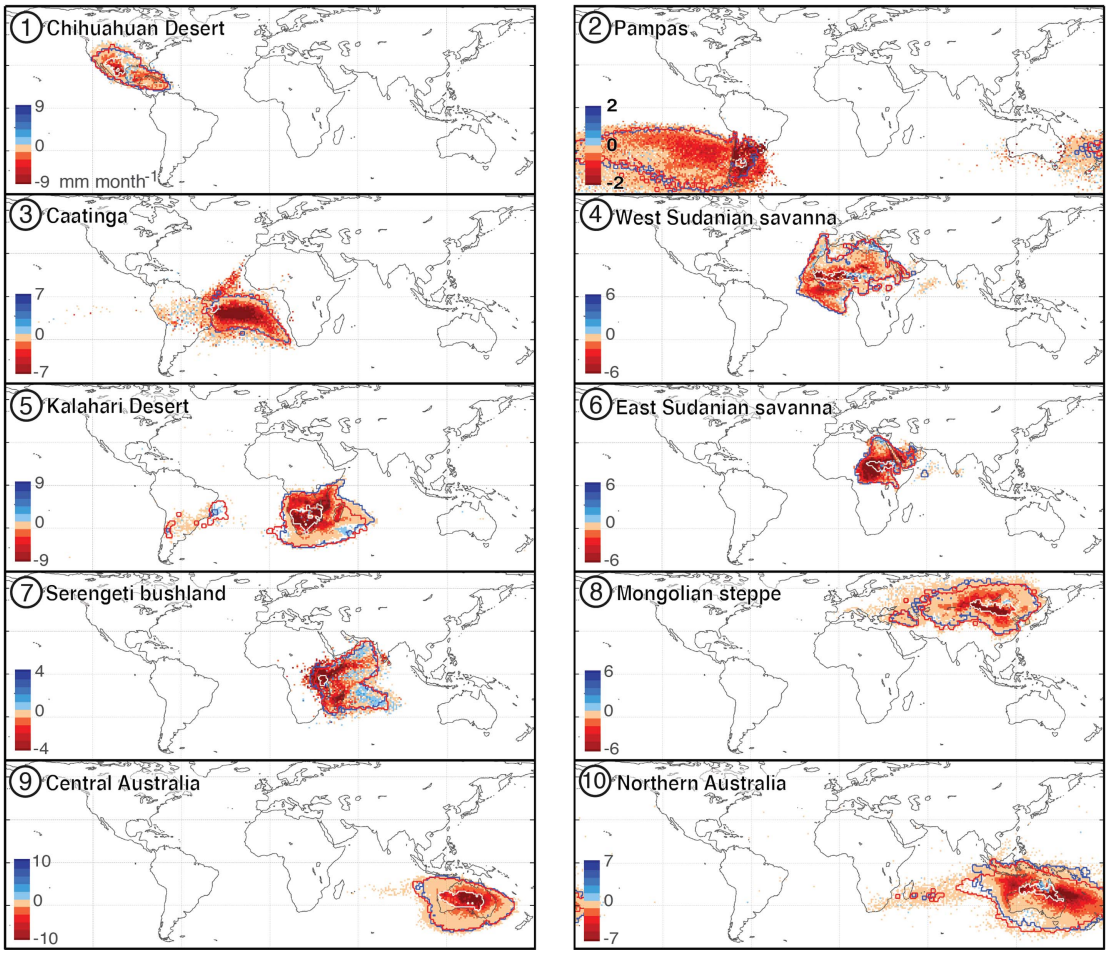

Figure 3. Regions contributing precipitation to the ecoregions during wet and dry years. Background colors represent the differences in mm month^{-1} between the volumes of precipitation originated at each pixel during wet and dry growing seasons. Red pixels indicate where less precipitation originates in dry years than in wet years, blue pixels indicate the opposite. Blue/red contours represent the minimum area supplying 90% of the moisture entering the corresponding ecoregion during wet/dry growing seasons.

of vegetation species with different sensitivities to rainfall scarcity, and the existence of environmental or climatic controls other than the availability of water. As an example, although VOD values are similar in the Pampas grasslands and Northern Australian woodlands, the observed input of rainfall in the latter is more than seven times larger, both during wet and dry years.

Results in figure 2 indicate that the fraction of precipitation coming from oceanic and continental origin varies markedly from ecoregion to ecoregion. While the Pampas and Caatinga receive most of the precipitation from the Pacific and Atlantic oceans (respectively), others, such as the East Sudanian savanna and the Mongolian steppe, receive almost their entire supply from continental areas. These findings agree with previous studies pointing to central Asia and Sahel as two of the world's regions with largest dependency on continental-origin rainfall (Zeng *et al* 1999, Dirmeyer *et al* 2014). We note as well that in the case of the Pampas and Mongolian steppe, part of the input of moisture during the growing season may come through melting of snow and not from precipitation directly (Shinoda *et al* 2010, Havrylenko *et al* 2016), and that in regions such as Caatinga, a small fraction of the water supply may also come from irrigation (Siebert *et al* 2005). Figure 2 also shows that for each given ecoregion, the partitioning of precipitation between continental and oceanic origin remains similar during wet and dry years. This is in clear contrast to what could be expected if ocean evaporation dynamics alone were responsible for driving the anomalously wet and dry years, and suggests that land surface conditions help intensify wet and dry spells.

The strength of land–atmospheric coupling and the importance of regional evaporation for precipitation are often diagnosed by means of the recycling ratio (Eltahir and Bras 1996, Trenberth 1999), i.e. the volume of precipitation originated from regional evaporation over the total input of precipitation. Recycling ratios are usually larger for areas of high evaporation and low air advection, and tend to increase during convective seasons (Trenberth 1999). Precipitation recycling has been studied based on observational data (Eltahir and Bras 1996, Trenberth 1999), transport models (Numaguti 1999,

Dirmeyer and Brubaker 2007) and isotopes (Wright *et al* 2001), but comparisons between different studies are problematic due to the dependency on the scale of the study region (with recycling being 100% when considering the world as a whole, and 0% when considering a point domain). Based on our approach, we show that mean recycling ratios for the growing season vary substantially amongst the different ecoregions: from 3% recycling in the Pampas during wet years, up to 34% in the Kalahari Desert during dry years (figure 2). This range reflects to some extent the differences in area covered by each ecoregion but, undoubtedly, also the different role each ecoregion plays on its own climate (see section 5).

The location of the main sources of moisture to each ecoregion (see contours in figure 3) is in agreement with the expectations based on prevailing winds, and is in line with previous analyses of precipitation origin (Dirmeyer *et al* 2009, Keys *et al* 2012, Dirmeyer *et al* 2014, Gimeno 2014). As mentioned above, the relative contributions of oceanic- and continental-origin precipitation remain generally similar during wet and dry years (figure 2). However, when zooming into the specific source areas, we do observe local differences between wet and dry periods; red-coloured areas in figure 3 are responsible for an anomalously low contribution to the corresponding ecoregion's precipitation during the dry growing seasons, i.e. those are the areas from which the observed deficits in precipitation come from. We show that for ecoregions such as the Chihuahuan Desert—which harvests most of its rainfall from the surrounding land regions and from the Gulf of Mexico (Dirmeyer *et al* 2014)—the contribution of precipitation in dry years is homogeneously decreased across the entire source area. But for other ecoregions, restrictions in the supply of moisture in dry years come from very specific locations. In the case of Caatinga—which is watered from the equatorial Atlantic (Gimeno *et al* 2010a)—the difference mainly comes from a narrow offshore band south of the equator. For the Kalahari Desert and Central Australia—which are regions largely fed by rainfall of continental origin (Gimeno *et al* 2010a) (figure 2)—restrictions in the supply of moisture come from land areas surrounding the ecoregions, or even including them (figure 3).

4.2. Mechanisms driving the anomalies in water supply to the ecoregions

The observed inter-annual anomalies in precipitation volumes (figure 2) and origin (figure 3) can be a consequence of any of the following three mechanisms, or combinations of them: (a) a persistent anomaly in wind speed and/or direction that leads to a change in the location of the source area (e.g., in the case of dry years, part of the moisture that is normally brought into the ecoregion is steered towards other regions); (b) a positive or negative anomaly in the volume of moisture generated in the source area; (c) a particularly high (or low) atmospheric stability over the ecoregion (see e.g. Dirmeyer *et al* 2014). These mechanisms are schematically represented in figure 4(a). As might be expected, any large-scale condition affecting these three proximate mechanisms will also impact the occurrence and variability of precipitation, including modes of internal climate variability such as ocean–atmospheric oscillations (Trenberth *et al* 2003, Schubert *et al* 2016).

General patterns of atmospheric circulation typically show little inter-annual variability, since they are largely dominated by the persistent mode of prevailing easterlies, westerlies and trade winds (Gimeno *et al* 2010a, Keys *et al* 2014). As a consequence, the location of the upwind source areas is rather stable for most regions; only the Kalahari Desert and the Australian ecoregions show notable differences between dry and wet growing seasons in the areas the air comes from (figures 4(b), supplementary figure A1). Meanwhile, during the dry growing seasons, the average evaporation in the source area of most ecoregions is anomalously low according to the satellite-based evaporation retrievals (Yu 2007, Miralles *et al* 2011), in particular for the Pampas, Caatinga, Kalahari Desert and the Australian ecoregions (figure 4(c)). We also see declines in the ecoregions' evaporation during dry years; this is mainly the case for the Chihuahuan and Kalahari deserts, Australia and the Mongolian steppe (figure 4(c)). This finding agrees with the declining volumes of recycled rainfall found in our FLEXPART experiments (figure 2), and further supports the existence of a positive feedback during dry times: growing-season rainfall scarcity and subsequent vegetation water stress lead to declines in soil evaporation and transpiration, which further reduce precipitation supply. As expected, this reduction is stronger in ecoregions with a larger dependency on precipitation recycling (figure 2). This is exemplified in figure 5, which shows the temporal evolution of water fluxes during the driest and wettest growing seasons on record for the Kalahari and Northern Australia, two of the ecoregions with highest recycling ratios. For both regions, the driest years—which were reported as extraordinary drought events in both cases (White *et al* 2004, Masih *et al* 2014)—show a consistent decline in growing-season (December–February) precipitation and evaporation, and a reduction in their seasonal VOD and NDVI peaks (March). The observed reduction in ecoregions' evaporation in dry years coincides with a decline in the simulated contribution of the ecoregions to their own precipitation supply, even if their recycling ratios are higher during dry years (see also figure 2). For both ecoregions, the vast majority of growing-season evaporation comes from transpiration: 78% and 73% for the Kalahari, and 66% and 71% for Northern Australia, for the driest and wettest year (respectively).

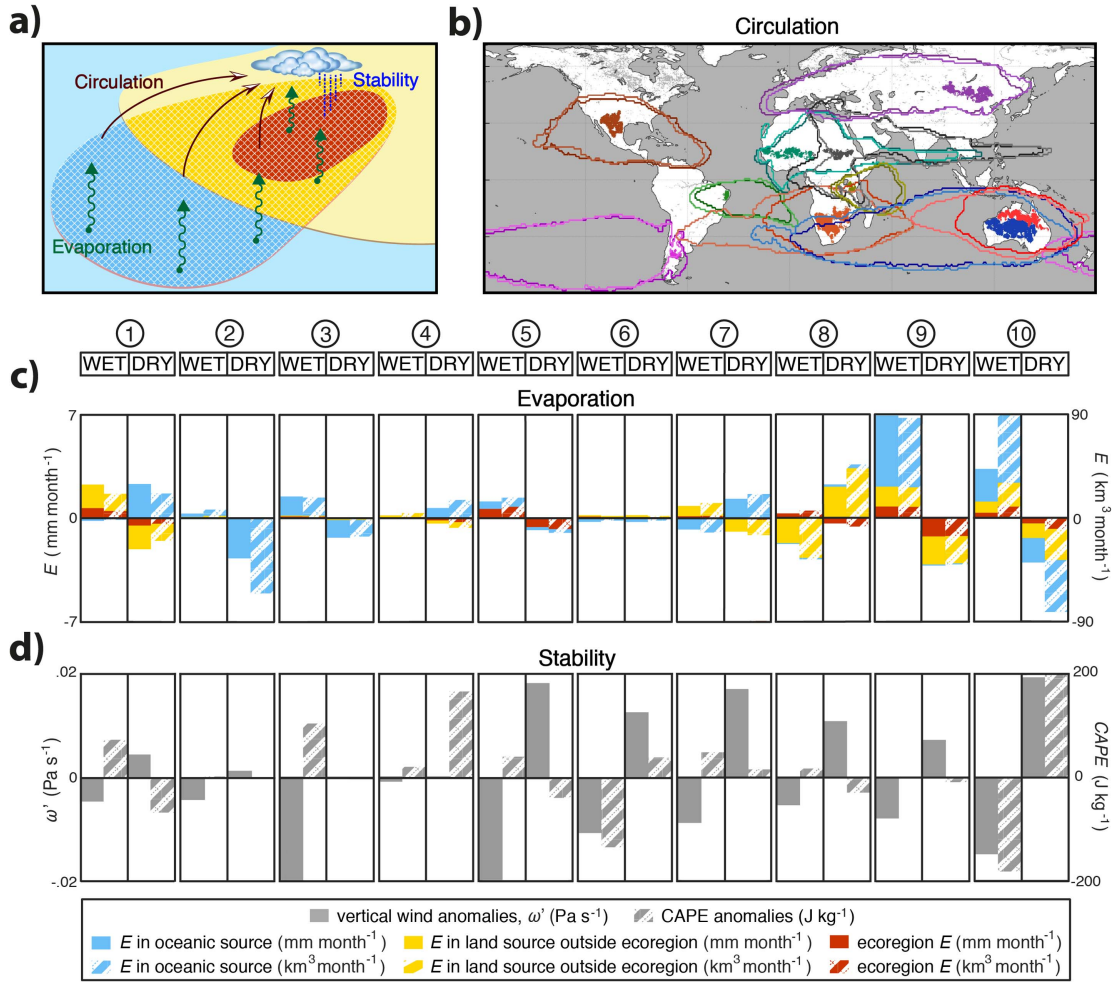

Figure 4. Immediate mechanisms driving the occurrence of wet and dry years. (a) Conceptual diagram of the three immediate physical mechanisms behind the differences in growing-season precipitation: atmospheric circulation, evaporation in the source region and local stability. (b) Mean growing-season atmospheric circulation: dark/light contours illustrate the origin of 90% of the air particles advected into each ecoregion for wet/dry years (according to the FLEXPART backward runs). Unlike the contours in figure 3, these areas do not depend on the gain or loss water vapour during the trajectories, thus are not directly influenced by evaporation. (c) Mean source evaporation (E) during wet and dry growing seasons, considering the overlap source region for dry and wet years (see contours in figure 3); results are presented as seasonal anomalies, in mm month^{-1} (full bars) and km^3 month^{-1} (stripped bars). The evaporation is illustrated separately for ocean (blue), land outside the ecoregion (yellow) and ecoregion (red). Ocean evaporation comes from OAFLUX and land evaporation from GLEAM. (d) Mean atmospheric stability during wet and dry growing seasons. Synoptic stability is diagnosed by the seasonal anomalies of vertical wind velocity at 500 hPa (ω')—with negative (positive) values indicating anomalously unstable (stable) atmosphere—and convective stability is diagnosed by anomalies in CAPE (J kg^{-1})—with negative (positive) values indicating anomalously low (high) convection. Stability data comes from ERA-Interim. All spatial averages are area-weighted.

Regardless of the fact that upwind evaporation and atmospheric circulation are defining the volume of atmospheric moisture present over an ecoregion, what finally controls whether that moisture precipitates is the instability of the atmosphere, i.e. the tendency to encourage the condensation and precipitation of that moisture. Figure 4(d) uses reanalysis data (Dee *et al* 2011) of 500 hPa vertical wind velocity anomalies (ω') to investigate mean synoptic stability—see e.g. Pampuch *et al* (2016), Gimeno *et al* (2010b)—and anomalies in CAPE to investigate mean convective stability—see e.g. Taylor and Ellis (2006), Johnson and Xie (2010). Overall, synoptic stability anomalies appear consistently relevant across all ecoregions, with the exception of the West Sudanian savanna. Mean stable conditions during the growing season are typical of years with limited input of precipitation and a reduced peak in vegetation biomass; anomalously unstable conditions are typical of years with a strong seasonal peak in biomass (figure 4(d)). This tendency occurs despite the fact that soil dryness may instigate convective instability through the warming of the lower troposphere (Taylor *et al* 2012, Guillod *et al* 2015), which agrees with the mean positive CAPE anomalies in regions such as the Sudanian savanna and Central Australia during dry years (figure 4(d)). In the examples of Kalahari and Northern Australia (figure 5), stable (unstable) synoptic conditions are found during the driest (wettest) growing season on record, while the effects of drier conditions on the average convection are only observed in the case of Northern Australia.

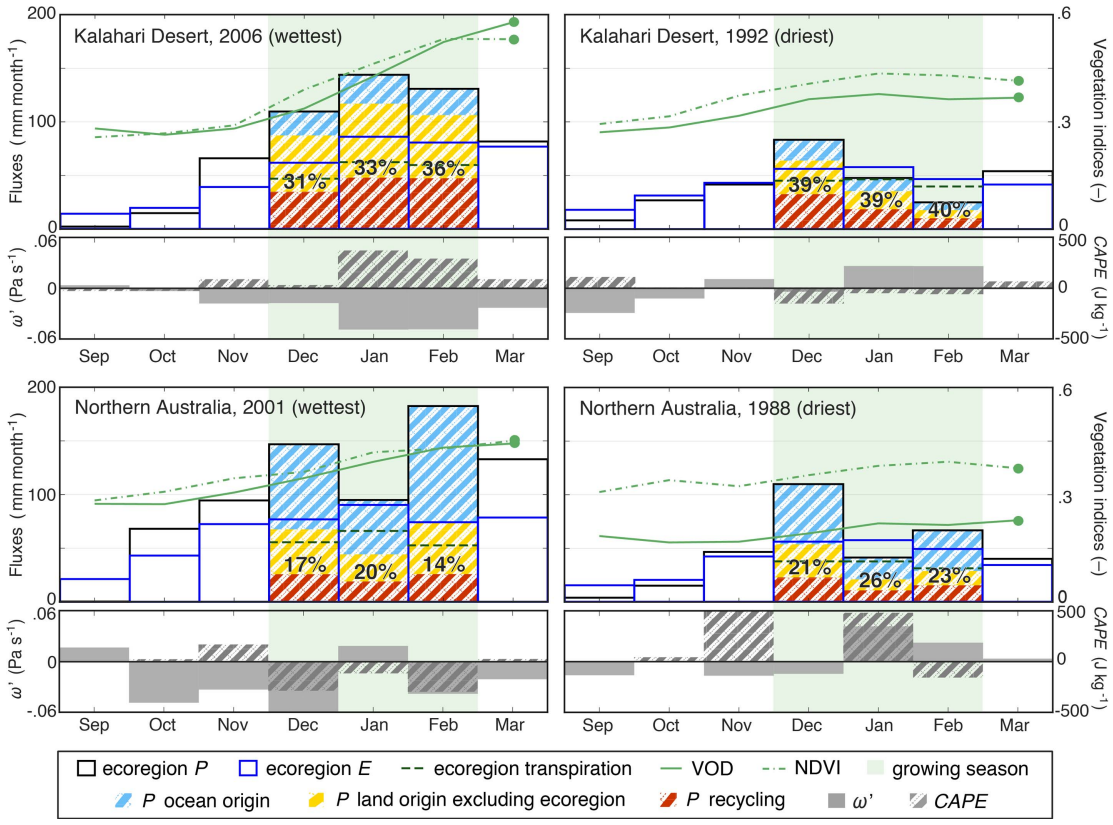

Figure 5. Driest and wettest years in Kalahari and Northern Australia. Vegetation dynamics (VOD, NDVI) and fluxes of evaporation (E) and precipitation (P) for these two ecoregions during the driest and wettest growing seasons on record (1980–2011). The contribution of the three possible precipitation sources is presented: oceanic origin (blue), land origin from outside the ecoregion (yellow), and the ecoregion itself (i.e. precipitation recycling, red). Seasonal anomalies vertical wind velocity at 500 hPa (ω') are used as a diagnostic of synoptic stability, and convective stability is diagnosed by anomalies in CAPE (J kg^{-1}). The transpiration (from GLEAM) is also noted. Recycling ratios are indicated in percentages. All spatial averages are area-weighted.

5. Discussion

Despite the inter-region contrasts in recycling, a common pattern is found in figure 2: although the total volumes of recycled moisture are lower during dry years, recycling ratios typically increase. This implies that the precipitation that originates from within the ecoregion does not decline as much as the volume of precipitation advected from outside the ecoregion during dry periods. This has already been suggested by previous studies, such as Bisselink and Dolman (2009). The decline in total volumes of precipitation recycled during dry times supports the overall positive sign of land feedbacks, which tend to intensify wet and dry conditions (Findell *et al* 2011, Guillod *et al* 2015). Conversely, the increase in recycling ratios backs the hypothesis that wet and dry spells are typically triggered by large-scale conditions that are external to the ecoregion (Schubert *et al* 2016), but also highlights the increased importance of local evaporation to sustain the input of precipitation during dry periods. Therefore, indirectly through transpiration, vegetation maintains a baseline supply of precipitation during periods of water stress (figure 5).

In addition, our results in figure 3 indicate that anomalies in the moisture generated and advected from neighbouring (or even remote) land regions can be responsible for a large fraction of the precipitation scarcity experienced by an ecoregion during dry years (see e.g. Kalahari or Central Australia). This implies that land-use change, wildfires, or the occurrence of wet and dry spells in these neighbouring (or remote) land areas, can thus be critical for the vegetation dynamics in the particular ecoregion that harvests rainfall from them (Keys *et al* 2012, Bagley *et al* 2014). This suggests the need to consider the impact of land management strategies in a given region, not just to maintain its own input of precipitation, but also to sustain the input of precipitation to remote regions that depend on the moisture generated in the former one (Keys *et al* 2012, 2014). This notion of teleconnected effects introduces a new dimension to traditional studies of the feedback of land on local rainfall (Taylor *et al* 2012, Guillod *et al* 2015).

From the three mechanisms conceptualised here as immediate causes of deficits in growing-season precipitation (figure 4(a)), changes in mean circulation do not seem significant compared to large-scale changes in evaporation and atmospheric stability. While the latter has been found relevant for all ecoregions,

atmospheric stability is linked to a plethora of factors acting on different scales. In extra-tropical latitudes, it mostly depends on baroclinic (synoptic) conditions, yet a large region can be baroclinicly stable and still contain thermodynamically (convective) unstable sub-regions. Therefore, it depends on all the processes affecting synoptic and convective conditions, e.g. the vertical profiles of air temperature, the atmospheric moisture content itself, or the soil moisture state (Betts and Ball 1998, Taylor and Ellis 2006). Nonetheless, we also show that the importance of the three factors in figure 4(a) varies markedly from region to region: while in ecoregions such as the Serengeti, higher-than-usual local atmospheric stability may on its own explain the reductions in growing-season precipitation and vegetation growth, in others, such as the Kalahari or Northern Australia, anomalies in evaporation, circulation and synoptic stability act together (figures 4(b)–(d), 5). A summary of the importance of these driving mechanisms for each ecoregion is presented in supplementary table A2. We also note that factors affecting cloud microphysics, such as changes in aerosol concentration (Ramanathan 2001), are not explicitly considered in this study.

Finally, while the three proximate mechanisms considered in figure 4(a) are conceptualised here separately, they are in fact to some degree inter-dependent, and they are also jointly affected by general climate variability patterns. Climate oscillations in particular —due to their associated preferential states in sea surface temperature and atmospheric pressure—can have important influences on atmospheric circulation, ocean and land evaporation, and atmospheric stability, all at the same time. Consequently, ocean–atmospheric teleconnections are expected to impact both precipitation and vegetation variability in these water-limited ecoregions (Myneni *et al* 1996, Miralles *et al* 2014b, Wright *et al* 2014, Gonsamo *et al* 2016). As an example, for the Caatinga and Kalahari Desert, all five wet years coincide with background La Niña conditions, while four out of the five dry years coincide with El Niño conditions; the latter also applies to the Central Australian ecoregion (not shown). These findings are in line with the expected dependence of global meteorological droughts on tropical Pacific sea surface temperatures (Trenberth *et al* 2013, Schubert *et al* 2016).

6. Conclusion

What drives precipitation in the most water-dependent ecoregions on Earth? While it is well known that large-scale sea surface temperatures and persistent atmospheric anomalies are essential to explain global precipitation extremes (Trenberth *et al* 2003, Schubert *et al* 2016), the input of rainfall into a land region finally depends on the volumes of water evaporated in the region and its surroundings, the atmospheric circulation of that moisture, and whether the stability profiles are suitable to yielding precipitation (Dirmeyer *et al* 2014). Here we have analysed the differences in the origin of rainfall during wet and dry years for ten global water-limited vegetated regions, using novel satellite observations and atmospheric trajectory modelling. Our results show that the factors driving the anomalies in growing-season precipitation vary strongly from ecoregion to ecoregion, and support the hypothesis that dry years are intensified by positive land–atmospheric feedbacks, yet only in regions of high precipitation recycling such as the Kalahari Desert or Australia (figure 2). Conversely, the precipitation originating from the ecoregion itself typically declines less in dry years than the volumes of precipitation advected from outside. This allows us to conclude that (a) wet and dry periods are initially triggered by conditions that are external to the ecoregion, yet (b) land feedbacks are overall positive, tending to intensify wet and dry conditions, and (c) the importance of local evaporation for the growth of vegetation becomes disproportionally large during dry times. The latter implies that, while transpiration is a net loss of water for the ecoregion, it can also be critical at maintaining a baseline supply of precipitation in periods of water stress. With water constraints predicted to aggravate in most of these ecoregions (Seneviratne *et al* 2012), further understanding of how vegetation and climate interact, what the impact of land management and restoration is on those interactions, and how to better characterise vegetation–climate feedbacks in Earth system models, appears critical to reliably estimate the fate of semi-arid regions and their role in future climate.

Acknowledgments

This work is funded by the Netherlands Organization for Scientific Research (NWO, grant 863.14.004) and the Belgian Science Policy Office (BELSPO) in the frame of the STEREO III programme project SAT-EX (SR/00/306). Raquel Nieto acknowledges funding by the Spanish MINECO within project TRAMO and the Galician Regional Government (Xunta) within project THIS, both co-funded by FEDER. Wouter Dorigo is supported by the personal grant TU Wien Science Award 2015. A J Dolman acknowledges funding by the Netherlands Earth System Science Center (NESSC). Diego G Miralles thanks Christopher Taylor, Brecht Martens and Mathieu Depoorter for the useful discussions.

Author contributions

Diego G Miralles, Raquel Nieto and Luis Gimeno conceived the study and designed the experiments. Diego G Miralles and Raquel Nieto conducted the analysis. Diego G Miralles wrote the paper. Yi Y Liu

provided the VOD data. All co-authors contributed to the editing of the manuscript, and the discussion and interpretation of the results.

References

Ahlström A *et al* 2015 The dominant role of semi-arid ecosystems in the trend and variability of the land CO_2 sink *Science* **348** 895–9

Andela N, Liu Y Y, van Dijk A I J M, de Jeu R A M and McVicar T R 2013 Global changes in dryland vegetation dynamics (1988–2008) assessed by satellite remote sensing: comparing a new passive microwave vegetation density record with reflective greenness data *Biogeosciences* **10** 6657–76

Bagley J E, Desai A R, Harding K J, Snyder P K and Foley J A 2014 Drought and deforestation: has land cover change influenced recent precipitation extremes in the Amazon? *J. Clim.* **27** 345–61

Betts A K and Ball J H 1998 FIFE surface climate and site-average dataset 1987–89 *J. Atmos. Sci.* **55** 1091–108

Bisselink B and Dolman A J 2009 Recycling of moisture in Europe: contribution of evaporation to variability in very wet and dry years *Hydrol. Earth Syst. Sci.* **13** 1685–97

Bonan G B 2008 Forests and climate change: forcings, feedbacks, and the climate benefits of forests *Science* **320** 1444–9

Casagrande E, Mueller B, Miralles D G, Entekhabi D and Molini A 2015 Wavelet correlations to reveal multiscale coupling in geophysical systems *J. Geophys. Res.: Atmos.* **120** 7555–72

Dee D P *et al* 2011 The ERA-Interim reanalysis: configuration and performance of the data assimilation system *Q. J. R. Meteorol. Soc.* **137** 553–97

Dirmeyer P A and Brubaker K L 2007 Characterization of the global hydrologic cycle from a back-trajectory analysis of atmospheric water vapor *J. Hydrometeorol.* **8** 20–37

Dirmeyer P A, Brubaker K L and DelSole T 2009 Import and export of atmospheric water vapor between nations *J. Hydrol.* **365** 11–22

Dirmeyer P A, Wei J, Bosilovich M G and Mocko D M 2014 Comparing evaporative sources of terrestrial precipitation and their extremes in MERRA using relative entropy *J. Hydrometeorol.* **15** 102–16

Drumond A, Marengo J, Ambrizzi T, Nieto R, Moreira L and Gimeno L 2014 The role of the Amazon Basin moisture in the atmospheric branch of the hydrological cycle: a Lagrangian analysis *Hydrol. Earth Syst. Sci.* **18** 2577–98

Eltahir E A B and Bras R L 1996 Precipitation recycling *Rev. Geophys.* **34** 367–78

Findell K L, Gentine P, Lintner B R and Kerr C 2011 Probability of afternoon precipitation in eastern United States and Mexico enhanced by high evaporation *Nat. Geosci.* **4** 434–9

Gimeno L 2014 Oceanic sources of continental precipitation *Water Resour. Res.* **50** 3647–9

Gimeno L, Drumond A, Nieto R, Trigo R M and Stohl A 2010a On the origin of continental precipitation *Geophys. Res. Lett.* **37** L13804

Gimeno L, Nieto R, Trigo R M, Vicente-Serrano S M and López-Moreno J I 2010b Where does the Iberian Peninsula moisture come from? An answer based on a Lagrangian approach *J. Hydrometeorol.* **11** 421–36

Gimeno L, Stohl A, Trigo R M, Dominguez F, Yoshimura K, Yu L, Drumond A, Durán-Quesada A M and Nieto R 2012 Oceanic and terrestrial sources of continental precipitation *Rev. Geophys.* **50** RG4003

Gonsamo A, Chen J M and Lombardozzi D 2016 Global vegetation productivity response to climatic oscillations during the satellite era *Glob. Change Biol.* **22** 3414–26

Guillod B P, Orlowsky B, Miralles D G, Teuling A J and Seneviratne S I 2015 Reconciling spatial and temporal soil moisture effects on afternoon rainfall *Nat. Commun.* **6** 1–6

Guswa A J, Celia M A and Rodríguez-Iturbe I 2004 Effect of vertical resolution on predictions of transpiration in water-limited ecosystems *Adv. Water Resour.* **27** 467–80

Harris I, Jones P D, Osborn T J and Lister D H 2013 Updated high-resolution grids of monthly climatic observations—the CRU TS3.10 dataset *Int. J. Clim.* **34** 623–42

Havrylenko S B, Bodoque J M, Srinivasan R, Zucarelli G V and Mercuri P 2016 Assessment of the soil water content in the Pampas region using SWAT *Catena* **137** 298–309

Jasechko S, Sharp Z D, Gibson J J, Birks S J, Yi Y and Fawcett P J 2013 Terrestrial water fluxes dominated by transpiration *Nature* **496** 347–50

Johnson N C and Xie S-P 2010 Changes in the sea surface temperature threshold for tropical convection *Nat. Geosci.* **3** 842–5

Keys P W, Barnes E A, van der Ent R J and Gordon L J 2014 Variability of moisture recycling using a precipitationshed framework *Hydrol. Earth Syst. Sci.* **18** 3937–50

Keys P W, van der Ent R J, Gordon L J, Hoff H, Nikoli R and Savenije H H G 2012 Analyzing precipitationsheds to understand the vulnerability of rainfall dependent regions *Biogeosciences* **9** 733–46

Koster R D, Dirmeyer P A, Guo Z, Bonan G, Chan E, Cox P, Gordon C, Kanae S, Kowalczyk E and Lawrence D 2004 Regions of strong coupling between soil moisture and precipitation *Science* **305** 1138–40

Liu Y Y, de Jeu R A M, McCabe M F, Evans J P and van Dijk A I J M 2011 Global long-term passive microwave satellite-based retrievals of vegetation optical depth *Geophys. Res. Lett.* **38** L18402

Liu Y Y, van Dijk A I J M, De Jeu R A M, Canadell J G, McCabe M F, Evans J P and Wang G 2015 Recent reversal in loss of global terrestrial biomass *Nat. Clim. Change* **5** 470–4

Liu Y Y, van Dijk A I J M, McCabe M F, Evans J P and De Jeu R A M 2013 Global vegetation biomass change (1988–2008) and attribution to environmental and human drivers *Glob. Ecol. Biogeogr.* **22** 692–705

Manfreda S and Caylor K 2013 On the vulnerability of water limited ecosystems to climate change *Water* **5** 819–33

Masih I, Maskey S, Mussá F E F and Trambauer P 2014 A review of droughts on the African continent: a geospatial and long-term perspective *Hydrol. Earth Syst. Sci.* **18** 3635–49

Miralles D G, Holmes T R H, De Jeu R A M, Gash J H, Meesters A G C A and Dolman A J 2011 Global land-surface evaporation estimated from satellite-based observations *Hydrol. Earth Syst. Sci.* **15** 453–69

Miralles D G *et al* 2016 The WACMOS-ET project: II. Evaluation of global terrestrial evaporation data sets *Hydrol. Earth Syst. Sci.* **20** 823–42

Miralles D G, Teuling A J, van Heerwaarden C C and Vilà-Guerau de Arellano J 2014a Mega-heatwave temperatures due to combined soil desiccation and atmospheric heat accumulation *Nat. Geosci.* **7** 345–9

Miralles D G *et al* 2014b El Niño–La Niña cycle and recent trends in continental evaporation *Nat. Clim. Change* **4** 122–6

Myneni R B, Los S O and Tucker C J 1996 Satellite-based identification of linked vegetation index and sea surface temperature Anomaly areas from 1982–1990 for Africa, Australia and South America *Geophys. Res. Lett.* **23** 729–32

Nemani R R 2003 Climate-driven increases in global terrestrial net primary production from 1982 to 1999 *Science* **300** 1560–3

Nieto R, Castillo R, Drumond A and Gimeno L 2014 A catalog of moisture sources for continental climatic regions *Water Resour. Res.* **50** 5322–8

Numaguti A 1999 Origin and recycling processes of precipitating water over the Eurasian continent: experiments using an atmospheric general circulation model *J. Geophys. Res.* **104** 1957–72

Olson D M and Dinerstein E 2001 Terrestrial ecoregions of the world: a new map of life on Earth a new global map of terrestrial ecoregions provides an innovative tool for conserving biodiversity *Bioscience* **51** 933–8

Owe M, De Jeu R A M and Holmes T R H 2008 Multisensor historical climatology of satellite-derived global land surface moisture *J. Geophys. Res.* **113** F01002

Pampuch L A, Drumond A, Gimeno L and Ambrizzi T 2016 Anomalous patterns of SST and moisture sources in the South Atlantic Ocean associated with dry events in southeastern Brazil *Int. J. Clim.* (doi:10.1002/joc.4679)

Poulter B *et al* 2014 Contribution of semi-arid ecosystems to interannual variability of the global carbon cycle *Nature* **509** 600–3

Ramanathan V 2001 Aerosols, climate, and the hydrological cycle *Science* **294** 2119–24

Rodriguez-Iturbe I, Porporato A, Laio F and Ridolfi L 2001 Plants in water-controlled ecosystems: active role in hydrologic processes and response to water stress: I. Scope and general outline *Adv. Water Resour.* **24** 695–705

Schubert S D *et al* 2016 Global meteorological drought: a synthesis of current understanding with a focus on SST drivers of precipitation deficits *J. Clim.* **29** 3989–4019

Seddon A W R, Macias-Fauria M, Long P R, Benz D and Willis K J 2016 Sensitivity of global terrestrial ecosystems to climate variability *Nature* **531** 229–32

Seibert P and Frank A 2004 Source-receptor matrix calculation with a Lagrangian particle dispersion model in backward mode *Atmos. Chem. Phys.* **4** 51–63

Seneviratne S I, Corti T, Davin E L, Hirschi M, Jaeger E B, Lehner I, Orlowsky B and Teuling A J 2010 Investigating soil moisture–climate interactions in a changing climate: a review *Earth Sci. Rev.* **99** 125–61

Seneviratne S I *et al* 2012 *Managing the Risks of Extreme Events and Disasters to Advance Climate Change Adaptation* ed C B Field *et al* (Cambridge: Cambridge University Press)

Shinoda M, Nachinshonhor G U and Nemoto M 2010 Impact of drought on vegetation dynamics of the Mongolian steppe: a field experiment *J. Arid Environ.* **74** 63–9

Siebert S, Döll P, Hoogeveen J, Faures J, Frenken K and Feick S 2005 Development and validation of the global map of irrigation areas *Hydrol. Earth Syst. Sci. Discuss.* **2** 1299–327

Spracklen D V and Garcia-Carreras L 2015 The impact of Amazonian deforestation on Amazon basin rainfall *Geophys. Res. Lett.* **42** 9546–52

Stohl A, Hittenberger M and Wotawa G 1998 Validation of the Lagrangian particle dispersion model FLEXPART against large-scale tracer experiment data *Atmos. Environ.* **32** 4245–64

Taylor C M, De Jeu R A M, Guichard F, Harris P P and Dorigo W A 2012 Afternoon rain more likely over drier soils *Nature* **489** 423–6

Taylor C M and Ellis R J 2006 Satellite detection of soil moisture impacts on convection at the mesoscale *Geophys. Res. Lett.* **33** L03404

Trenberth K 1999 Atmospheric moisture recycling: role of advection and local evaporation *J. Clim.* **12** 1368–81

Trenberth K E, Dai A, Rasmussen R M and Parsons D B 2003 The changing character of precipitation *Bull. Am. Meteorol. Soc.* **84** 1205–17

Trenberth K E, Dai A, van der Schrier G, Jones P D, Barichivich J, Briffa K R and Sheffield J 2013 Global warming and changes in drought *Nat. Clim. Change* **4** 17–22

Tucker C J, Pinzon J E, Brown M E, Slayback D A, Pak E W, Mahoney R, Vermote E F and El Saleous N 2005 An extended AVHRR 8 km NDVI dataset compatible with MODIS and SPOT vegetation NDVI data *Int. J. Remote Sens.* **26** 4485–98

White R P and Nackoney J 2003 *Drylands, People, and Ecosystem Goods and Services: A Web-Based Geospatial Analysis* (Washington: World Resources Institute)

White W B, Gershunov A, Annis J L, McKeon G and Syktus J 2004 Forecasting Australian drought using Southern Hemisphere modes of sea-surface temperature variability *Int. J. Clim.* **24** 1911–27

Wright C K, de Beurs K M and Henebry G M 2014 Land surface anomalies preceding the 2010 Russian heat wave and a link to the North Atlantic oscillation *Environ. Res. Lett.* **9** 1–10

Wright W E, Long A and Comrie A C 2001 Monsoonal moisture sources revealed using temperature, precipitation, and precipitation stable isotope timeseries *Geophys. Res. Lett.* **28** 787–90

Wu D, Zhao X, Liang S, Zhou T, Huang K, Tang B and Zhao W 2015 Time-lag effects of global vegetation responses to climate change *Glob. Change Biol.* **21** 3520–31

Yu L 2007 Global variations in oceanic evaporation (1958–2005): the role of the changing wind speed *J. Clim.* **20** 5376–90

Zeng N, Neelin J D, Lau K M and Tucker C J 1999 Enhancement of interdecadal climate variability in the Sahel by vegetation interaction *Science* **286** 1537–40

Zhao M and Running S W 2010 Drought-induced reduction in global terrestrial net primary production from 2000 through 2009 *Science* **329** 940–3